Published in "Scattering and Surface Roughness III", Z.-H. Gu and A. A. Maradudin, Editors, Proc. SPIE 3784, 304-313 (1999).

Multidetector hemispherical polarized optical scattering instrument

Thomas A. Germer

Optical Technology Division
National Institute of Standards and Technology
Gaithersburg, MD 20899

ABSTRACT

A multidetector optical scattering instrument is described and characterized. The instrument has twenty-eight detectors surrounding and substantially covering the scattering hemisphere. Each detector contains a polarizer so that each is only sensitive to p-polarized scattered light. The polarization of the incident light is linear and can be rotated into any angle. With this instrument, polarized light scattering measurements can be performed in multiple directions at once. The utility of this instrument is demonstrated by measuring the light scattered from a microrough silicon sample and silicon surfaces containing different sizes of polystyrene latex spheres. The results are compared to the predictions of theoretical calculations. It is shown that the distribution of polarization parameters for each of the different sizes of spheres and for microroughness are different. It is expected that designs similar to the one presented here will allow for improved on-line characterization of defects on smooth surfaces.

Keywords: defect detection, instrumentation, optical scatter, polarimetry, surface inspection

1. INTRODUCTION

Recent research results have found that when polarized light is incident upon a bare wafer, which has particulate contamination, subsurface defects, or microroughness, the light scattered into different directions has a signature polarization, which can be used to identify the source of scatter.[1–4] For example, light scattered by roughness in the smooth-surface limit has a polarization that is independent of the random surface height function.[2,4–7] This finding allows the development of microroughness-blind scattering instruments, which can improve sensitivity of detection of small defects and particles.[8] The light scattered by interfacial roughness in dielectric layers is also polarized, if the correlation between those roughness functions is high.[9–11] Other work has shown polarization of light scattered by particulate contaminants can be used to estimate their sizes.[3,12]

Previous polarized optical scatter measurements by our group have concentrated on measurements using a weakly focused laser beam and a goniometer to manipulate a high-angular-precision collection system.[13,14] Samples have all contained delocalized sources of scatter, such as roughness, or large ensembles of defects, such as particles and subsurface defects. The weak focusing of the incident laser beam, while allowing for higher angular resolution, limits the minimum spot size with which one can illuminate the sample.

In order to complement our current instrumentation capabilites, and to demonstrate a practical application of the research findings, we have designed a prototype light scattering surface inspection instrument. By utilizing twenty-eight polarization-sensitive scattered light collection systems, this instrument can capture a snapshot of the light scattering function and part of its polarization behavior. Operation of this instrument consists of using the integrated intensity of scattered light to locate defects on a surface, and then using the signals from each detector for different incident polarizations to characterize each defect. It is expected that instruments such as this will improve the ability for surface inspection instruments to perform rapid "on-the-fly" characterization of defects on semiconductor fabrication lines and other manufacturing environments.

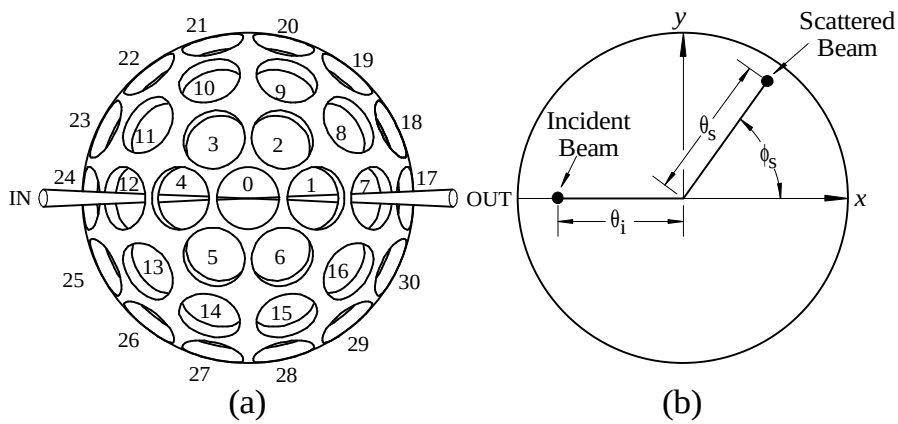

Figure 1 (a) Top view of the hemispherical detector holder, showing the different detector ports, the location of the incident beam entrance port, and the location of the specular beam exit port; and (b) the coordinate system, shown as projections of unit vectors onto a plane parallel to the sample surface, used to describe incident and scattering directions.

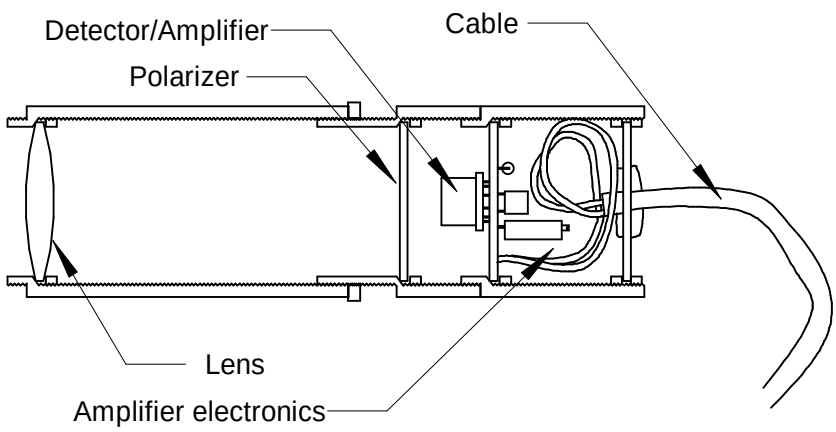

Figure 2 Cross sectional view of a detection system, showing the locations of the relay lens, polarizer, detector/amplifer, amplifier electronics, and cable.

It is the purpose of this article to describe and demonstrate the Multidetector Hemispherical Polarized Optical Scattering Instrument (MHPOSI). In Section 2, details of the instrument will be given, and in Section 3, operation of the instrument will be demonstrated by using it to analyze scatter from microrough silicon and polystyrene latex (PSL) spheres on silicon. Some concluding remarks will be made in Section 4.

2. INSTRUMENT DESCRIPTION

Figure 1(a) shows a top view of the MHPOSI collection shell, upon which are mounted twenty-eight detection systems. The shell consists of a hemisphere of inner radius 65 mm, with 3 mm removed from its open end. Thus, the thirty-one ports, numbered 0 through 30, are each aligned to a point 3 mm beyond the edge of the shell. One port (Port 0) is used for a retractable low power microscope with a ×6 objective. Another port (Port 12) is used for the incident beam optics, while a third (Port 7) is left open to allow the specularly reflected laser beam to exit the system. The remaining twenty-eight ports hold detection systems. The collection half-angle is approximately

TABLE 1 The direction of the center of each port on MHPOSI.

Port	θ	ϕ	Port	θ	ϕ
1	24°	0	16	49°	324°
2	24°	60°	17	74°	0°
3	24°	120°	18	74°	26°
4	24°	180°	19	74°	51°
5	24°	240°	20	74°	77°
6	24°	300°	21	74°	103°
7*	49°	0°	22	74°	129°
8	49°	36°	23	74°	154°
9	49°	72°	24	74°	180°
10	49°	108°	25	74°	206°
11	49°	144°	26	74°	231°
12**	49°	180°	27	74°	257°
13	49°	216°	28	74°	283°
14	49°	252°	29	74°	309°
15	49°	288°	30	74°	334°

*Port left open for exit of specular beam
**Port used for incident laser beam.

10° for each port, corresponding to a collection solid angle of about 0.1 sr. Therefore, the twenty-eight detection ports cover about 2.8 sr or about 45 % of the scattering hemisphere.

Figure 1(b) shows the coordinates used to describe the incident and scattering directions. The incident and scattering polar angles, θ_i and θ_s, are defined with respect to the sample normal, and the azimuthal scattering angle ϕ_s is defined with respect to the plane of incidence. The azimuthal incident angle ϕ_i is assumed to be 180° throughout this study. Light that is s-polarized has its electric field perpendicular to the direction of propagation and the sample normal, and light which is p-polarized has its electric field in the plane defined by the direction of propagation and the sample normal. Table I lists the central directions of each port of MHPOSI.

Figure 2 shows one of the twenty-eight collection system which are mounted onto the hemispherical shell. The units are constructed from modular stackable lens tubes (Thorlabs SM1 Series[†]). A BK7 biconvex antireflection-coated 35 mm focal length lens is used to image the sample illumination spot onto a detector. An absorbing thin film polarizer (Edmund Scientific) is mounted between the lens and the detector and can be rotated for alignment. The detector consists of a Si photodetector/amplifier package (UDT Sensors UDT-455/UV) with a 5 mm diameter circular detection region. The detector is mounted on a circular printed circuit board containing feedback elements necessary to achieve a 1 GΩ transimpedance, bandwidth-limiting capacitors, and a trim potentiometer. Since the optics are approximately one-to-one imaging, the field of view at the sample is about 5 mm in diameter. The electrical power to the amplifier electronics and the amplified signal are carried by a multiconductor cable to and from a computer interface and power supply. At this time, the absolute response of the detectors has not been calibrated.

Light from an Argon ion laser (35 mW, 488 nm) passes through a computer-controlled mechanical shutter, beam expanding optics, and neutral density filters before being aligned onto the sample. A nematic liquid crystal polarization rotator (Meadowlark Optics), preceded by a Glan-laser polarizer, allows computer control of the

[†] Certain commercial equipment, instruments, or materials are identified in this paper in order to specify the experimental procedure adequately. Such identification is not intended to imply recommendation or endorsement by the National Institute of Standards and Technology, nor is it intended to imply that the materials or equipment identified are necessarily the best available for the purpose.

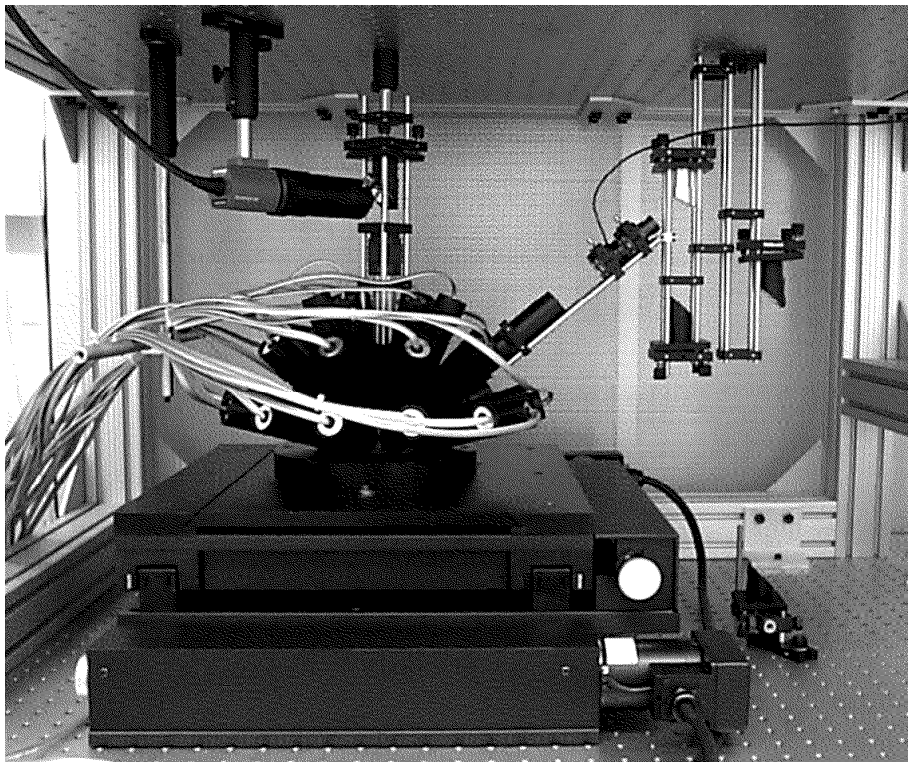

Figure 3 A photograph of the Multidetector Hemispherical Polarized Optical Scatter Instrument.

incident linear polarization state. A 75 mm focal length achromatic lens, located on a lens tube attached to the hemispherical shell (Port 12) is used to focus the laser beam onto the sample. This lens is nominally 75 mm from the sample, so that a collimated laser beam is focused at the sample. The spot size of the laser, however, is variable, determined by adjusting the beam expanding optics. The smallest spot size at the sample is on order of 5 μm in the direction tranverse to beam propagation direction. Thus, at an incident angle of 49°, the spot on the sample is elliptical with major axes of approximately 5 μm and 8 μm.

Figure 3 shows a photograph of the instrument. The hemispherical shell is suspended from an inverted optical breadboard held above an xy translation stage using modular aluminum extrusion. The entire instrument is housed in a laminar horizontal-flow class 10 clean hood. The sample translation stage (Aerotech ATS32020) has 200 mm of motion along two axes with 1 μm resolution and 4 μm accuracy. The sample is secured to a vacuum chuck on the translation stage.

Data are collected by a 16 bit 100 kHz data acquisition board (Kiethley-Metrabyte DAS-1802HR-DA) with two multiplexing expansion boards (Kiethley-Metrabyte EXP-1800). This configuration allows collection of all the signals from 30 detectors in an interval of 0.3 ms. In order to improve the signal-to-noise ratio, and since the rate limiting operation of the instrument is currently control of the sample stage motion and switching of the incident polarization state, the signal is typically averaged over a number of interleaved measurements (typically 30 for the signal and 300 for background measurements). A background signal, achieved by periodically closing a shutter on the laser (usually at the end of each line scan in an image), is also measured. The signals are also normalized by a reference signal, picked off the incident beam, to account for laser fluctuations.

Focusing of the laser beam at the sample is performed by lowering the microscope objective and adjusting the beam expanding telescope to minimize laser spot size on a highly scattering, but nondiffusive, sample, such

as an etched backside of a silicon wafer. This position of the telescope is noted, and larger spots can be achieved by widening the two elements of the telescope, thus bringing the focus closer to the incident beam focusing lens.

The alignment of the polarizer in each lens tube was accomplished by marking the lens tube with the pass direction, determined in a separate setup before each collection system is mounted onto the hemispherical shell. Once the collection systems were mounted onto the hemispherical shell, the assembly was viewed from the top. Each lens tube was then adjusted so that the mark was visually aligned along the radial direction. In this manner, the polarizers are aligned to pass p-polarized light with an accuracy of about 5 degrees. Note that rotation of the polarizer is coupled to focusing of the scattered light onto the detector (see Fig. 2); however, since the detector is large compared to the focused spot size, this focusing is not critical. The incident beam polarizer was aligned so that its rejected beam was vertical in the laboratory. Manufacturer-calibrated voltages were used for the liquid crystal polarization rotator.

At each point on the sample, the signals for four incident linear polarization states are measured [0° (s), 45°, 90° (p), and 135°]. Images are then made by scanning the sample under the fixed laser beam, with line scans carried out in the x-direction. The signal $S_i(\alpha)$ for the i-th detector with the incident light polarized at an angle α (with respect to s-polarized), after background subtraction and normalization by the reference signal, are then saved to disk. The effective intensity signal for the i-th detector is determined from

$$\bar{I}^{(\mathrm{p})}(i) = [S_i(0°) + S_i(45°) + S_i(90°) + S_i(135°)]/2.$$

The effective intensity $\bar{I}^{(\mathrm{p})}(i)$ is the signal one would measure if unpolarized light were incident upon the sample. The direction of incident linear polarization which maximizes the p-polarized light scattering into the i-th detector is given by

$$\bar{\eta}^{(\mathrm{p})}(i) = \arctan[S_i(45°) - S_i(135°), S_i(0°) - S_i(90°)]/2,$$

where $\arctan(x, y)$ is the two argument arc tangent, which preserves the quadrant of the point (x, y). The degree to which the signal for the i-th detector changes as the incident polarization is rotated is given by

$$\bar{P}_{\mathrm{L}}^{(\mathrm{p})}(i) = \{[(S_i(0°) - S_i(90°)]^2 + [(S_i(45°) - S_i(135°)]^2\}^{1/2}/\bar{I}_i^{(\mathrm{p})}$$

The parameters $\bar{I}^{(\mathrm{p})}$, $\bar{\eta}^{(\mathrm{p})}$, and $\bar{P}_{\mathrm{L}}^{(\mathrm{p})}$ are referred to as *inverse* bidirectional ellipsometry parameters. These parameters are similar to the bidirectional ellipsometry parameters, $I^{(\mathrm{p})}$, $\eta^{(\mathrm{p})}$, and $P_{\mathrm{L}}^{(\mathrm{p})}$, used in previous work by our group,[1–4,9,12] except that they correspond to the incident light polarization which scatters into p-polarized light, rather than the polarization of scattered light when p-polarized light is incident on the sample.

3. RESULTS

A. Microroughness

To test the operation of the instrument with a rough sample, we used the MHPOSI to measure the scatter from a microfabricated silicon microroughness standard consisting of a pseudorandom distribution of circular pits with nominal diameters of 1.31 μm and 1.76 μm and nominal depths of 10 nm.[15] Use of this sample ensured that the material had a well-defined surface microroughness, with negligible particulate contamination or subsurface features. Previous measurements have shown that the scattering from this sample follows the predictions of first-order vector perturbation theory to a high degree.[2,4]

The MHPOSI measurements were taken on the microrough silicon sample, averaged over a 20 mm x 20 mm area. The results are shown in Fig. 4. In order to compare these results to first-order vector perturbation theory,[6,7] integrated scatter calculations were carried out using a nominal power spectral density function. Details of these calculations are found elsewhere in the literature.[16] The discrepancies are probably a result of a combination of the imperfect alignment of each of the detector polarizers and the incident polarization rotator, as well as

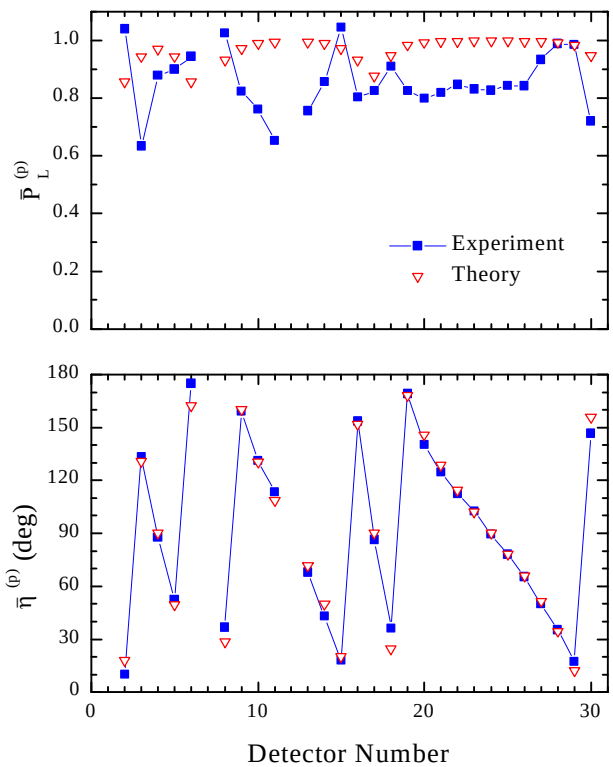

Figure 4 The spatially-averaged inverse bidirectional ellipsometry parameters as functions of detector number for a microrough silicon sample. The solid squares correspond to experimental data, and the open triangles correspond to predictions from first-order vector perturbation theory.

the uncertainties in the modeling, due to the parameterization of the sample power spectrum. The agreement between the theory and experiment, however, is qualitatively very good.

B. Particulate Contaminants

Recent measurements and theoretical calculations have demonstrated that the polarization of light scattered by dielectric spheres on silicon surfaces can be used to estimate the size of spherical particles.[3,12] The theory found that predictions in three different approximations, including the Rayleigh, Mie-surface, and the discrete dipole approximations, were similar for small and medium angle scattering. This finding suggested that particle size can be determined for a much wider class of contaminants than spheres, and that one does not need to know the material of the sphere to determine its size.

Using an electrostatic deposition system, polystyrene latex spheres having diameters 101 nm, 181 nm, and 217 nm were deposited onto bare silicon wafers.[17] Wafers containing relatively high surface number densities (2000–5000 mm^{-2}) of PSL spheres were used to demonstrate the instrument's sensitivity and discrimination capabilities. The densities used for these measurements were chosen so that most of the spheres were just resolved from one another. Figure 5 shows the image of $\sum_i \bar{I}^{(\mathrm{p})}(i)$ (i chosen to be those detectors which are not adjacent to the specular beam: 2–6, 9-11, 13–15, and 18–30) for the 101 nm spheres and for p-polarized incident

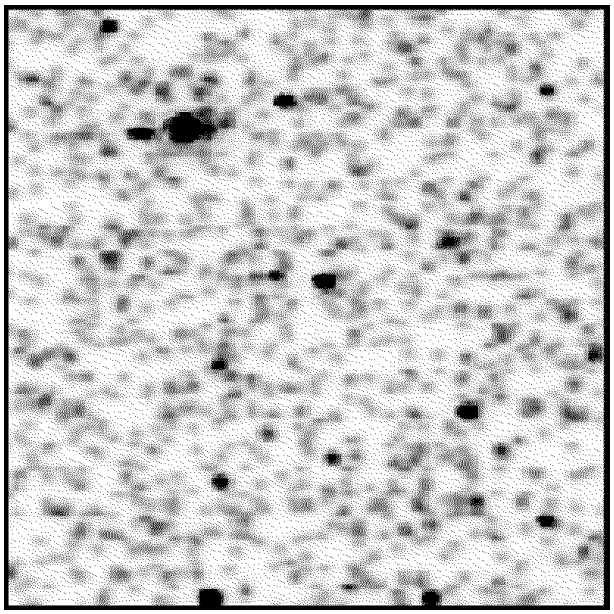

Figure 5 Scanned integrated scatter image showing 100 nm polystyrene latex (PSL) spheres on silicon. The scan area is 0.5 mm × 0.5 mm (200 × 200 pixels). The image has a negative intensity scale.

light, showing clearly resolved features having roughly equal integrated amplitude. A few bright spots can be seen in Fig. 5, which are due to foreign particles, doublets, or multiple isolated spheres in the illuminated region.

Images of $\bar{\eta}^{(\mathrm{p})}(i)$ and $\bar{P}_{\mathrm{L}}^{(\mathrm{p})}(i)$ do not show substantial contrast between the spheres, since the sphere density is high enough that the signal is dominated by the spheres even at large illumination-sphere separations. Contrast exists in several locations on each wafer, presumably due to the presence of the uncharacterized defects mentioned above. These defects are usually, but not always, associated with particularly bright spots on the wafers. When it is associated with particularly bright spots, the polarimetric signature extends far beyond the size of the laser spot.

Five areas, each containing approximately 50 particles and few foreign particles, were chosen on each wafer for signal averaging and for extraction of $\bar{\eta}^{(\mathrm{p})}(i)$ and $\bar{P}_{\mathrm{L}}^{(\mathrm{p})}(i)$. Figure 6(a) shows the results of this analysis for the three sphere sizes. The statistical uncertainty in the results are indicated by the spread in the data. The absolute uncertainty has not been completely determined, since both the incident and scattered polarizations have not been extensively calibrated. However, such absolute uncertainties are expected to only have minor effects on our conclusions.

Theoretical calculations based upon the discrete dipole approximation are shown with the data.[18,19] The signals were calculated for the central angles for each detector, and did not include an integration over the solid angle of each detector. The results of these calculations are shown in Fig. 6(b). Qualitative agreement exists between the theory and the experiment; however, quantitatively there are substantial differences. In particular, the values of $\bar{\eta}^{(\mathrm{p})}$ for detectors 18–30 ($\theta_{\mathrm{s}} = 74°$) follow the same trend as the particle size is increased; however the magnitude of the deviation of $\bar{\eta}^{(\mathrm{p})}(i)$ from 90° is not well predicted by the theory. Whether these differences are a result of innaccuracies in the theoretical calculations, or indications of some systematic error in the measurements, is not known at this time.

Despite the differences between the theory and the measurement, it is clear from Fig. 6 that the three different sphere sizes can be distinguished by the MHPOSI. The values of $\bar{\eta}^{(\mathrm{p})}(i)$ and $\bar{P}_{\mathrm{L}}^{(\mathrm{p})}(i)$, where i is the

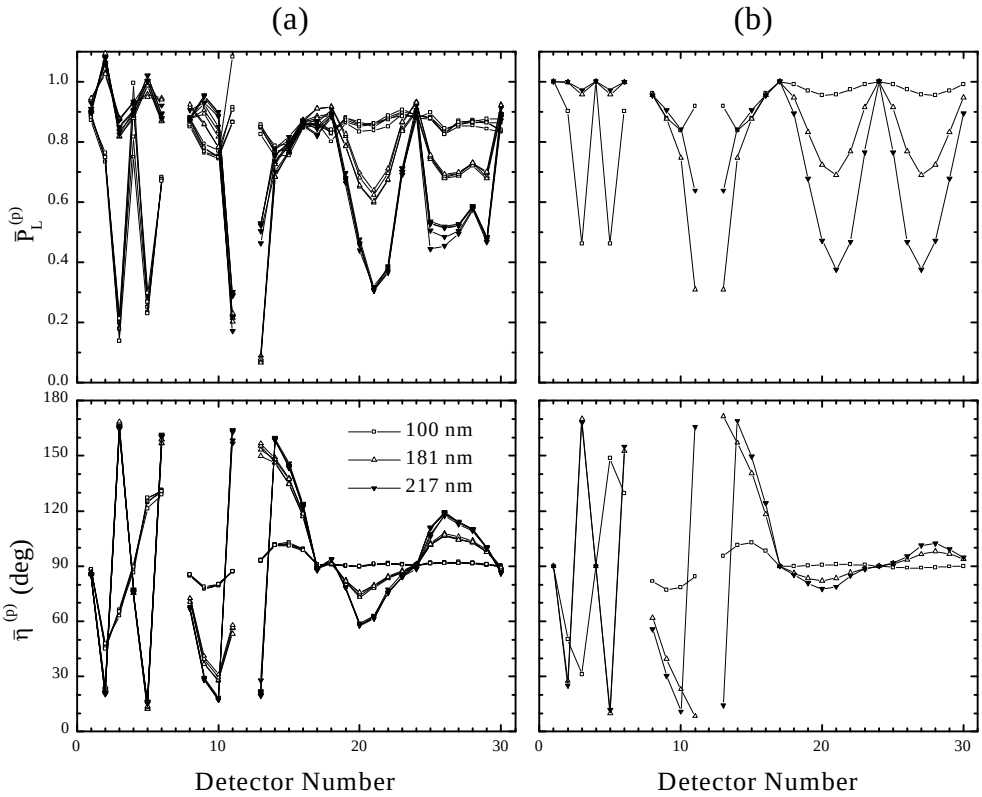

Figure 6 The spatially-averaged inverse bidirectional ellipsometry parameters, $\bar{\eta}^{(\mathrm{p})}(i)$ and $\bar{P}_{\mathrm{L}}^{(\mathrm{p})}(i)$, as functions of detector number for 101 nm, 181 nm, and 217 nm diameter PSL spheres on silicon. On the left are experimental data, and on the right are results of discrete dipole calculations.

detector number are also significantly different than those obtained for the microrough silicon sample, suggesting that distinguishing between roughness and particles is possible using this technique.

4. CONCLUDING REMARKS

The instrument described in this paper was designed to demonstrate that polarimetric measurements in multiple simultaneous directions can be used to rapidly characterize local defects on smooth surfaces. The use of multiple scattering detectors improves the ability of the instrument to make distinctions between different scattering sources by providing some redundancy in the measurement, and by providing more degrees of freedom for resolving the differences between different types of defects. While this paper emphasized the agreement between the measurements and theoretical calculations, it is expected that pattern recognition techniques would enhance the capabilities of the instrument by allowing a much wider range of defect types to be detected and analyzed. For example, a neural network may be employed by the analysis software to allow the instrument to learn the characteristic patterns for $\bar{I}^{(\mathrm{p})}(i)$, $\bar{\eta}^{(\mathrm{p})}(i)$, and $\bar{P}_{\mathrm{L}}^{(\mathrm{p})}(i)$ for each type of defect encountered on a production line. Perhaps a commercial implementation of this instrument would include not only a database of known defects but the ability to interface with defect management software to allow the correlation between defects characterized by various tools. As off-line tools, such as scanning electron microscopes (SEM), characterize the defects found on

the light scattering tool, the light scattering tool would learn to recognize those defects which it has encountered before, reducing the need for off-line characterization.

ACKNOWLEDGEMENTS

The author would like to thank Dr. Lipiin Sung and Dr. George Mulholland for assistance in the deposition of PSL spheres on wafers and Bradley Scheer of VLSI Standards, Inc., for supplying the microrough silicon sample.

REFERENCES

[1] T. A. Germer, "Angular dependence and polarization of out-of-plane optical scattering from particulate contamination, subsurface defects, and surface microroughness," Appl. Opt. **36**, 8798–8805 (1997).

[2] T. A. Germer, C. C. Asmail, and B. W. Scheer, "Polarization of out-of-plane scattering from microrough silicon," Opt. Lett. **22**, 1284–1286 (1997).

[3] L. Sung, G. W. Mulholland, and T. A. Germer, "Polarization of light scattered by particles on silicon wafers," in *Surface Characterization for Computer Disks, Wafers, and Flat Panel Displays*, J. C. Stover, ed., Proc. SPIE **3619**, 80–91 (1999).

[4] T. A. Germer, and C. C. Asmail, "Polarization of light scattered by microrough surfaces and subsurface defects," J. Opt. Soc. Am. A **16**, 1326–1332 (1999).

[5] M. D. Williams, and D. E. Aspnes, "Polarimetry of specular and non-multiple-scattered electromagnetic radiation from selectively roughnened Si surfaces," Phys. Rev. Lett. **41**, 1667–1670 (1978).

[6] D. E. Barrick, *Radar Cross Section Handbook*, (Plenum, New York, 1970).

[7] S. O. Rice, "Reflection of Electromagnetic Waves from Slightly Rough Surfaces," Comm. Pure and Appl. Math. **4**, 351–378 (1951).

[8] T. A. Germer, and C. C. Asmail, "Microroughness-blind hemispherical optical scatter instrument," U.S. Patent Application #09/058,182 (April 10, 1998).

[9] T. A. Germer, "Application of bidirectional ellipsometry to the characterization of roughness and defects in dielectric layers," in *Flatness, Roughness, and Discrete Defect Characterization for Computer Disks, Wafers, and Flat Panel Displays II*, J. C. Stover, ed., Proc. SPIE **3275**, 121–131 (1998).

[10] J. M. Elson, "Light scattering from surfaces with a single dielectric overlayer," J. Opt. Soc. Am. **66**, 682–694 (1976).

[11] J. M. Elson, "Multilayer-coated optics: guided-wave coupling and scattering by means of interface random roughness," J. Opt. Soc. Am. A **12**, 729–742 (1995).

[12] L. Sung, G. W. Mulholland, and T. A. Germer, "Polarization of light scattered by spheres on silicon," Opt. Lett. , in press (1999).

[13] T. A. Germer, and C. C. Asmail, "Goniometric optical scatter instrument for out-of-plane ellipsometry measurements," Rev. Sci. Instr. , in press (1999).

[14] T. A. Germer, and C. C. Asmail, "A goniometric optical scatter instrument for bidirectional reflectance distribution function measurements with out -of-plane and polarimetry capabilities," in *Scattering and Surface Roughness*, Z.-H. Gu, and A. A. Maradudin, ed., Proc. SPIE **3141**, 220–231 (1997).

[15] B. W. Scheer, "Development of a physical haze and microroughness standard," in *Flatness, Roughness, and Discrete Defect Characterization for Computer Disks, Wafers, and Flat Panel Displays*, J. C. Stover, ed., Proc. SPIE **2862**, 78–95 (1996).

[16] T. A. Germer, and C. C. Asmail, "Proposed methodology for characterization of microroughness-induced optical scatter instrumentation," in *Flatness, Roughness, and Discrete Defect Characterization for Computer Disks, Wafers, and Flat Panel Displays*, J. C. Stover, ed., Proc. SPIE **2862**, 12–17 (1996).

[17] G. W. Mulholland, and M. Fernandez, "Accurate Size Measurement of Monosize Calibration Spheres by Differential Mobility Analysis," in *Characterization and Metrology for ULSI Technology*, D. G. Seiler, W. M. Bullis, A. C. Diebold, R. McDonald, and T. Shaffner, ed., Proc. AIP **449**, 819–823 (1998).

[18] R. Schmehl, B. M. Nebeker, and E. D. Hirleman, "Discrete-dipole approximation for scattering by features on surfaces by means of a two-dimensional fast Fourier transform technique," J. Opt. Soc. Am. A **14**, 3026–3036 (1997).

[19] B. M. Nebeker, G. W. Starr, and E. D. Hirleman, "Modeling of Light Scattering from Structures with Particle Contaminants," in *Flatness, Roughness, and Discrete Defect Characterization for Computer Disks, Wafers, and Flat Panel Displays*, J. C. Stover, ed., Proc. SPIE **2862**, 139–150 (1996).